

First-principles study of nucleation, growth, and interface structure of Fe/GaAsSteven C. Erwin,^{1,2} Sung-Hoon Lee,^{2,*} and Matthias Scheffler²¹Center for Computational Materials Science, Naval Research Laboratory, Washington, D.C. 20375²Fritz-Haber-Institut der Max-Planck-Gesellschaft, Faradayweg 4–6, D-14195 Berlin-Dahlem, Germany

(Received 27 December 2001; published 22 May 2002)

We use density-functional theory to describe the initial stages of Fe film growth on GaAs(001), focusing on the interplay between chemistry and magnetism at the interface. Four features appear to be generic: (1) At submonolayer coverages, a strong chemical interaction between Fe and substrate atoms leads to substitutional adsorption and intermixing. (2) For films of several monolayers and more, atomically abrupt interfaces are energetically favored. (3) For Fe films over a range of thicknesses, both Ga and As adlayers dramatically reduce the formation energies of the films, suggesting a surfactantlike action. (4) During the first few monolayers of growth, Ga or As atoms are likely to be liberated from the interface and diffuse to the Fe film surface. Magnetism plays an important auxiliary role for these processes, even in the dilute limit of atomic adsorption. Most of the films exhibit ferromagnetic order even at half-monolayer coverage, while certain adlayer-capped films show a slight preference for antiferromagnetic order.

DOI: 10.1103/PhysRevB.65.205422

PACS number(s): 75.70.-i, 82.65.+r, 75.50.Bb, 72.25.Mk

I. INTRODUCTION

Magnetic materials are widely anticipated to be integrated into semiconductor-based microelectronics during the next decade or two.¹ A major component of this effort has focused on using ferromagnetic thin films as a source for creating spin-polarized electrical current in a semiconductor substrate, a process referred to as “spin injection.” Three criteria have been identified as important for technologically useful spin injection: (1) substantial spin polarization of the injected current; (2) electrons, rather than holes, serving as the spin-polarized carriers; and (3) Curie temperatures for the source of order room temperature or higher.

Although several materials appear to meet one or two of these criteria, none has yet met all three. Several diluted magnetic semiconductors based on Be and Mn doping of ZnSe^{2,3} and Mn doping of GaAs⁴ have recently demonstrated spin-injection efficiencies of greater than 50%, but only near liquid helium temperatures. Other magnetic semiconductors, including CdCrSe, can be doped both *p* and *n* type and have Curie temperatures of order 100–200 K,⁵ but their performance as spin-injection sources has yet to be examined.

In addition to the magnetic semiconductors, much current research continues to focus on one of the earliest studied candidate materials, Fe.⁶ Besides offering the possibility of room-temperature injection of electron spins, Fe has the potential advantage of forming a nearly lattice-matched epitaxial film on an important semiconductor substrate, GaAs. However, despite this early promise and after considerable research investment, measured spin-injection efficiencies for Fe/GaAs remain frustratingly low, typically no larger than 1%.^{7,8} The reason for this low efficiency is not definitively known, and much controversy surrounds its origin. A crucial issue, not yet settled, is whether the measured efficiencies reflect an intrinsic upper limit or are simply due to technical limitations that may be overcome or circumvented. For example, much early effort focused on the nature of interface layers inferred to be “magnetically dead,” in the sense that

they do not contribute to the total magnetic moment of the Fe film.^{9,10} The appearance of dead layers is consistent with the formation (thermodynamically favorable in the bulk) of nonmagnetic FeAs complexes at an interface with the As-rich GaAs(001)-(2×4) surface. This reasoning led to the development of two strategies for suppressing As diffusion into the Fe film: passivation of the As-rich surface by a surfactant such as sulfur¹¹ and growing on the *Ga-rich* GaAs(001)-(4×6) surface (or, equivalently, As decapping prior to growth).¹² Both approaches lead to films with magnetization onset in the range 4–8 monolayers (ML) and with essentially the full moment per Fe atom in all layers.^{12–14}

Notwithstanding the successful elimination of dead layers, measured spin-injection efficiencies have, until recently, remained at or below the 1% level. Recently, Schmidt *et al.* have argued that a more fundamental limitation exists for spin injection from a ferromagnetic metal into a semiconductor.¹⁵ They have shown that in the purely diffusive regime (where spins are scattered much less frequently than electrons) the spin-injection efficiency from a ferromagnet (fm) into a semiconductor (sc) is proportional to the ratio of their conductivities, σ_{sc}/σ_{fm} . For ferromagnetic metals this ratio is of order 10^{-4} and for typical device geometries suggests maximum injection efficiencies of 1% or less.

There remain several possibilities for circumventing this limitation on Fe sources. The first is to operate in the ballistic regime, where the contact resistance due to elastic backscattering at the interface (Sharvin resistance) will generally reduce the metal-semiconductor conductivity mismatch.¹⁵ Tang *et al.* have used concepts from mesoscopic transport to model injection into a two-dimensional electron gas and find clear evidence for ballistic spin transport that otherwise vanishes in the diffusive limit.¹⁶

A second possibility, relevant to the diffusive regime, is the use of tunnel contacts at the Fe/GaAs interface, which are expected to substantially reduce the conductivity mismatch and thereby increase the injection efficiency.¹⁷ Related research avenues concern the role of intrinsic Schottky barriers

in controlling the spin-dependent tunneling through an interface.¹⁸ Indeed, Zhu *et al.* have recently demonstrated injection from Fe into GaAs with an efficiency of about 2% at room temperature; they suggest that the Schottky barrier formed between Fe and GaAs leads to a tunnel contact, thus circumventing the problems of conductance mismatch.¹⁹ Very recently, Hanbicki *et al.* have used a Schottky contact to an AlGaAs overlayer to inject spin into GaAs with efficiencies of 30% at low temperature and 9% at room temperature.²⁰

Since the prospects and limitations for spin injection from Fe into GaAs remain uncertain, we believe that further progress may benefit from a first-principles theoretical description of the interface. Our focus will be on the atomic structure of the interface and its resultant magnetic character, especially during the first few monolayers of growth. Theoretical studies of buried interfaces are notoriously difficult, for several reasons. First, experimental probes can provide only indirect information about physical and electronic structure, and hence are of limited utility for guiding theories. Moreover, real interfaces may—even after careful annealing—have atomic geometries very different from the ground state; hence, the interface structure may depend on the precise growth history. In principle, one approach to this dilemma would be first-principles finite-temperature molecular dynamics simulation of film growth, which would properly account for the roles of deposition rate, surface diffusion, and incorporation into the substrate. In practice, molecular dynamics using density-functional theory can at best simulate processes for ~ 100 ps—many orders of magnitude short of the experimentally relevant time scales, which may be milliseconds or longer. Kratzer and Scheffler have recently addressed this problem using a “first-principles kinetic Monte Carlo” method.²¹ However, the complexity of applying this method to the growth of Fe on GaAs—with three atomic species and many different possible processes—makes such an approach not yet feasible.

In this paper we approach the problem from two different limits. In Sec. II we consider the initial stages of interface formation, beginning with adsorption of isolated Fe adatoms on a bare GaAs substrate. We focus here on the potential-energy surface governing surface diffusion and show that Fe-As chemistry may play a decisive role in the submonolayer regime. In Sec. III we consider a different limit: namely, the thermodynamic ground-state interface structure of Fe films several monolayers thick. Here we concentrate on the magnetic character of the interface as a function of film thickness and propose a mechanism that accounts for the experimentally observed delayed onset of ferromagnetic order for films of a few monolayers.^{12,14,22} In Sec. IV we discuss ways to reconcile our results from these two limiting regimes, and we propose future directions for further study.

II. INITIAL STAGES OF GROWTH

Our goal in this section is to identify and quantify those structural, magnetic, and chemical features that may be *generic* to the growth of Fe on GaAs. We do not attempt a

definitive treatment of growth on a particular GaAs reconstruction or at a particular temperature. Instead, we focus on the following four questions: (1) Does the initial adsorption of atomic Fe prefer metallic bonding at highly coordinated sites, or does covalent bonding to Ga or As prevail? (2) Does adsorbed Fe nucleate the formation of compact islands, or do adsorbate-substrate interactions dominate the growth? (3) Is surface diffusion of Fe likely to be significant at growth temperatures? (3) Are the Fe magnetic moments in the submonolayer regime governed by strong Hund coupling (atomic moments) or by itinerancy effects (bulk moments)?

We begin by studying Fe adsorption on a fictitious, but chemically reasonable, surface of GaAs(001): namely, a (2×1) reconstruction consisting of bulk GaAs terminated by a dimerized Ga layer. This fictitious surface is analogous to the dimerized $\beta(2 \times 4)$ and $\beta 2(2 \times 4)$ As-rich surfaces, but is quite different from the more complex $\zeta(4 \times 2)$ surface believed to be the basis for the $c(8 \times 2)$ reconstruction observed under Ga-rich conditions.²³

We use density-functional theory together with the generalized gradient approximation (GGA) for the exchange-correlation functional.²⁴ For the calculations in this section we used Troullier-Martins pseudopotentials and a plane-wave basis with a kinetic-energy cutoff of 50 Ry, as implemented in the FHI96MD code.²⁵ The sampling of the surface Brillouin zone was equivalent to using 64 k points for a (1×1) surface unit cell.

To construct the potential-energy surface (PES) for adsorption of atomic Fe on a clean surface, we computed the total energy, E_t , as a function of the adsorbate position (X, Y) within the surface unit cell. To minimize interactions of the adsorbate with its periodic images we used a (2×2) supercell. For each adsorbate position (X, Y) , we fully relaxed the Z coordinate of the adsorbate and the positions of all Ga and As atoms in the top two layers of the surface. This procedure was repeated for adsorbate positions sufficient to sample the PES with a resolution of about 0.25 Å. For many adsorbate positions, geometries with subsurface adsorption or with atomic positions exchanged were considered as well; in each case, the lowest-energy configuration was used to define $E_t(X, Y)$.

In order to illuminate the detailed role—if any—of magnetism in the adsorption energetics, we begin by first calculating the PES without allowing for spin polarization. We then recalculate the PES while allowing for spin polarization and examine the differences that arise. If the adsorbate moment were completely localized and did not interact with the substrate, these two energy surfaces would be identical except for an overall shift of the energies. Thus, the differences that we find (described below) directly reflect site-dependent magnetic interactions between the Fe moment and the GaAs substrate.

Figure 1 shows the PES calculated without spin polarization, for a portion of the surface unit cell shown in Fig. 2. We restrict the plot to the vicinity of the dimer rows because the energy landscape between dimer rows is quite flat and considerably higher in energy. Along the dimer rows the PES is periodic with repeat length $a/\sqrt{2}$. Figure 1 shows slightly more than one full period along this direction.

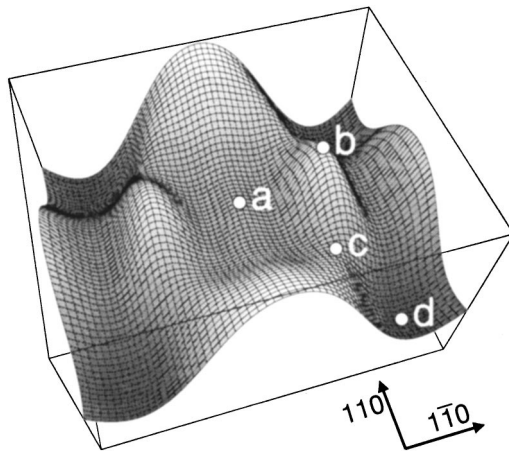


FIG. 1. Potential-energy surface for Fe on GaAs(001), calculated using GGA without spin polarization. The labeled points correspond to the configurations in Fig. 2.

Each point on this PES corresponds to a different relaxed geometry, determined solely by the in-plane adsorbate position (X, Y) . We focus on the four points marked in Fig. 1, which correspond to the four geometries shown in Fig. 2. Point (a), in the center of the PES, corresponds to adsorption at the high-symmetry pedestal site, midway between two dimers along a dimer row. Although this site is highly coordinated, leading to four Fe-Ga and two Fe-As bonds of nearly equal length (2.5 Å), it is energetically unfavorable. Indeed, this site is not even locally metastable: energy is gained by moving the adsorbate in any direction away from point (a).

The global minimum of the PES is a point (d) near the corner of the region shown in Fig. 1. This is 0.8 eV below point (a) and corresponds to the configuration of Fig. 2(d), in which the Fe adsorbate has partially “kicked out” one Ga atom from a surface dimer and taken its place. The large energy gain from this process suggests that the formation of such Fe-Ga heterodimers may act as a strong local trap for Fe, strongly suppressing surface diffusion of the Fe adatoms. If the kicked-out Ga atom subsequently diffuses away to a more stable adsorption site, this trapping effect will be further enhanced. Such effects, if not kinetically hindered, will bias the growth toward nucleating many small Fe islands.

The issue of kinetic barriers to forming Fe-Ga heterodimers can be analyzed by considering the possible routes leading to point (d) along the PES. For example, the reaction pathway from point (a) to (d) proceeds via point (c), which corresponds to the configuration shown in Fig. 2(c). This is the transition state (the highest energy configuration along the minimum-energy pathway) for the reaction taking (a) into (d), and is only 0.25 eV higher than the valley floor near (a). Part of this barrier arises from breaking the original Ga-Ga dimer bond, but apparently most of this energy cost is recovered by forming a more stable Fe-Ga heterodimer bond. Another 1.0 eV is recovered at point (d) by forming, in addition, a new Fe-As backbond to the substrate. The kicked-out Ga atom may remain bonded to the Fe atom, but it is energetically much more favorable to break this Fe-Ga bond

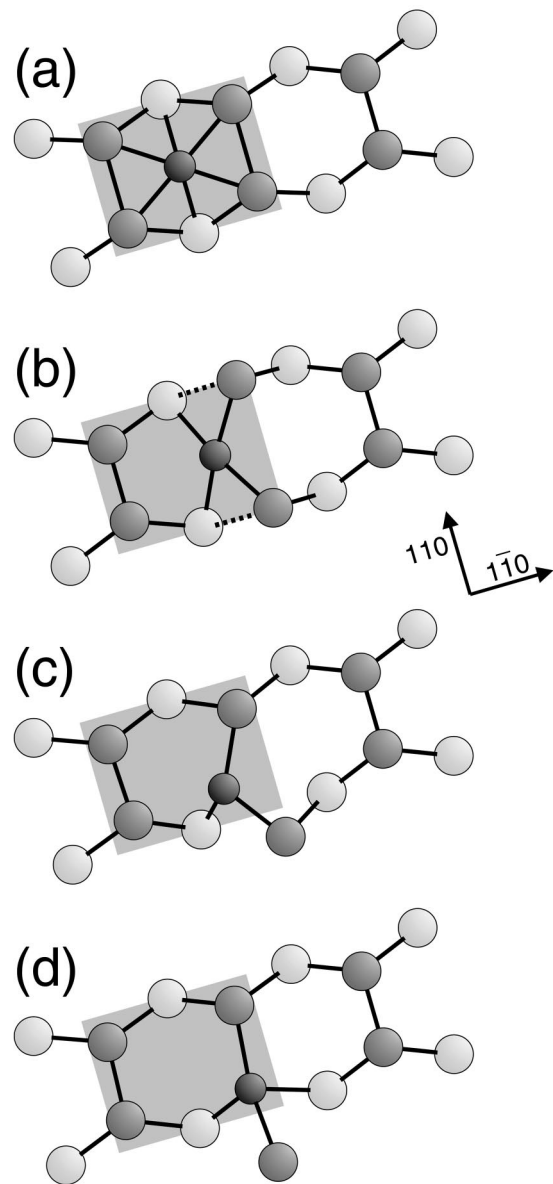


FIG. 2. Relaxed configurations for Fe adsorbed at the four locations marked in Fig. 1. The gray and light gray spheres represent Ga and As atoms, and the smaller dark gray spheres represent Fe atoms. Highly strained bonds (in the range 15%–20% longer than bulk) are shown as dotted lines. The shaded area marks the region for which the potential-energy surface is plotted in Fig. 1.

(at a cost of 0.6 eV) and diffuse to a more favorable binding site—for a net gain up to 2.0 eV per Ga atom for the limiting case of incorporation into bulk Ga. Comparing these energy changes upon bond breaking, we conclude that Fe-As bonds are considerably more stable than Fe-Ga bonds.

The final adsorbate site we discuss is point (b), halfway between the pedestal site and the dimer bridge site. At this point, the Ga-Ga dimer bond has already broken to allow for more favorable Fe-Ga bonds to begin forming. Without spin polarization, the energy of this configuration is a local maximum and represents a strong barrier to breaking Ga-Ga dimer bonds head on. A similar barrier is found for a Fe adatom artificially constrained to approach the Ga-Ga dimer

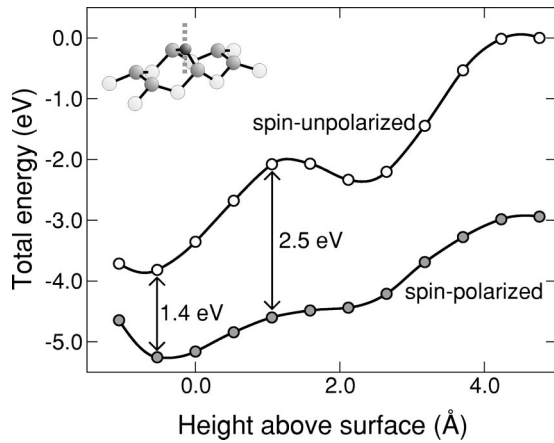


FIG. 3. Relative total energy for Fe constrained to approach the Ga-dimer bridge site from directly above, as shown. Energies are with respect to the spin-unpolarized energy for Fe far above the GaAs surface. The vertical distance between the two curves is the magnetic energy gain. Without spin polarization there is a local barrier of ~ 0.4 eV for breaking the Ga dimer; when spin polarization is included this barrier is removed.

from directly above, as shown in Fig. 3. For this adsorption route from above, an energy cost of ~ 0.4 eV must be paid before the Ga-Ga dimer bond finally breaks; once paid, stable Fe adsorption can occur at the bridge site.

We turn now to the differences in the PES that arise from including spin polarization. We have repeated the calculation of the entire PES using spin-polarized GGA, allowing for any changes in the relaxed geometries. In general, we find only negligible changes to the relaxed atomic positions, and so the geometries shown in Fig. 2 continue to correspond to points on the new PES, shown in Fig. 4. Comparing the spin-unpolarized and spin-polarized energy landscapes (Figs. 1 and 4), several features deserve comment. The global minimum is the same for both, corresponding to the Fe-Ga heterodimer formation via Ga “kick-out.” With spin polarization, the pedestal site is again unstable against adsorbate motion in any direction.

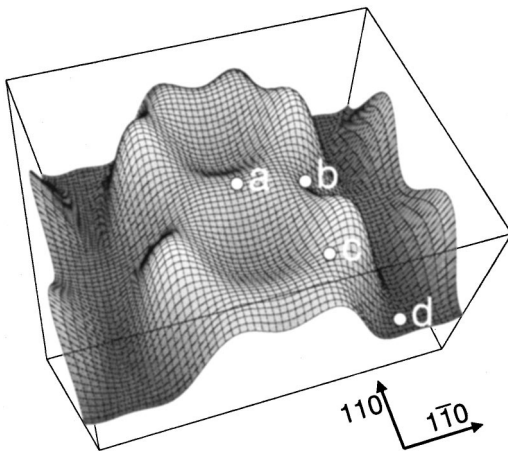


FIG. 4. Potential-energy surface for Fe on GaAs(001), calculated with spin polarization. The labeled points are the same as in Fig. 1 and correspond very closely to the configurations in Fig. 2.

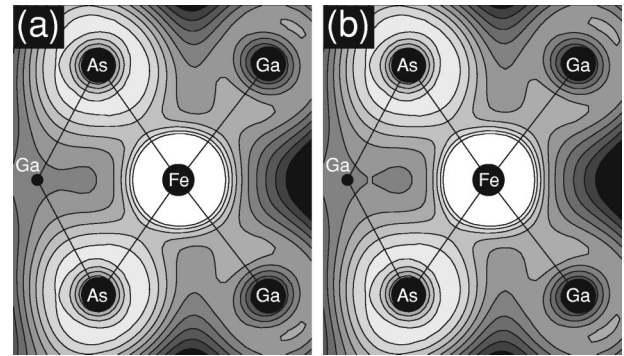


FIG. 5. Comparison of the (a) spin-unpolarized and (b) spin-polarized valence electron densities near the Fe atom for the configuration shown in Fig. 2(b). The contours are logarithmically spaced; lighter contours represent higher density and are truncated near the Fe atom. Projected atomic positions are marked by black circles; their size indicates proximity to the plotting plane.

Differences are also apparent. The spin-polarized energy surface appears more corrugated; this is due almost entirely to a strong reduction of energies near point (b) (a local maximum without spin polarization) and the nearby dimer bridge site (a saddle point without spin polarization, but part of a low-energy trench with it). Thus by including spin polarization, the barrier to head-on Ga-Ga dimer breaking is reduced to zero. The same difference is observed in dimer breaking by a Fe atom artificially constrained above the dimer: the barrier in Fig. 3 is eliminated by including spin polarization—demonstrating that this effect is not limited to surface diffusion.

To understand why allowing for spin polarization changes some parts of the PES but not others, we consider two plausible explanations: chemical effects and magnetic effects. By the former we mean contributions to the total energy that depend primarily on the total valence electron density; by the latter we mean contributions related to the electron spin density. We focus on the configuration of Fig. 2(b), for which the change in the PES is particularly dramatic. In Fig. 5 we compare the spin-unpolarized and spin-polarized total valence-electron density in a plane containing the Fe adsorbate and its As and Ga neighbors. In both plots, Fe-As and Fe-Ga bonds are clearly visible, and the loss of both the Ga-Ga dimer bond and the Ga-As backbond is obvious. Most importantly, there are no large differences between the spin-polarized and unpolarized electron densities in this plane. We conclude that the changes in the PES due to spin polarization cannot be attributed to changes in the valence-electron density related to chemical bonds.

To evaluate the role of magnetic effects in determining the shape of the PES, we first consider how the total magnetic moment per cell varies with the Fe adsorbate position. In Fig. 6 we show the magnetic energy (the difference between spin-polarized and unpolarized energies), as a function of total magnetic moment, for about 50 different adsorption sites on the PES. Most of the sites have magnetic moments between $2\mu_B$ and $3\mu_B$, giving rise to magnetic energies between 0.4 and 0.8 eV. About ten sites have considerable higher moments, between $3.2\mu_B$ and $3.4\mu_B$, and corre-

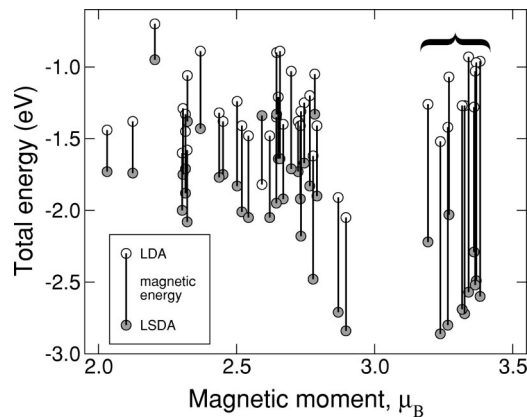


FIG. 6. Relative total energies for a number of configurations used to define the potential-energy surfaces in Figs. 1 and 4. The configurations within the bracket are all located near point (b) in Figs. 1 and 4 (see text for discussion).

spondingly higher magnetic energies, between 1.0 and 1.6 eV. Thus these sites, all located near point (b) on the PES, give rise to large differences in the spin-polarized and unpolarized energy landscapes. These differences can be attributed to the development of unusually large magnetic moments for adsorption sites in the vicinity of energy barriers in the spin-unpolarized PES; these sites generally involve highly strained or partially broken bonds. The same trend is observed for the constrained adsorption from above (Fig. 3). The magnetic energy gain at the configuration corresponding to the barrier is 2.5 eV, nearly twice as large as at the equilibrium adsorbate height. This difference again arises from the difference in magnetic moments: $3.9\mu_B$ at the barrier configuration versus $3.2\mu_B$ at equilibrium. Thus we conclude that magnetic effects play an important role in determining those parts of the PES corresponding to highly strained or partially broken bonds.

We end this section by turning briefly to another process important during growth: the adsorption of Fe in the presence of preadsorbed Fe. We consider 1/4 monolayer of Fe in its lowest-energy configuration, i.e., incorporated as Fe-Ga heterodimers with (2×2) periodicity. To simplify the discussion, we assume a starting surface from which the kicked-out Ga atoms have detached and diffused away. We then recalculate the (spin-polarized) potential-energy surface for this preadsorbed surface, again fully accounting for geometrical relaxation.

A portion of this PES is shown in Fig. 7(a), along with the initial preadsorbed surface structure in Fig. 7(b). The area shown is roughly twice that of Fig. 4, and a general comparison of the corresponding portions reveals the following. First, the overall corrugation of the preadsorbed PES is smaller than for the clean surface; i.e., preadsorbed Fe lowers the barriers to surface diffusion. The locations on this PES labeled (e)–(h) correspond to global minima on the PES of the clean surface. Point (e), located at the position of the preadsorbed Fe, is here a local energy maximum. This suggests that Fe-Fe bonding is not yet favorable in this low coverage regime, at least relative to the further formation of Fe-Ga heterodimers. Points (f)–(h) are local minima, indicat-

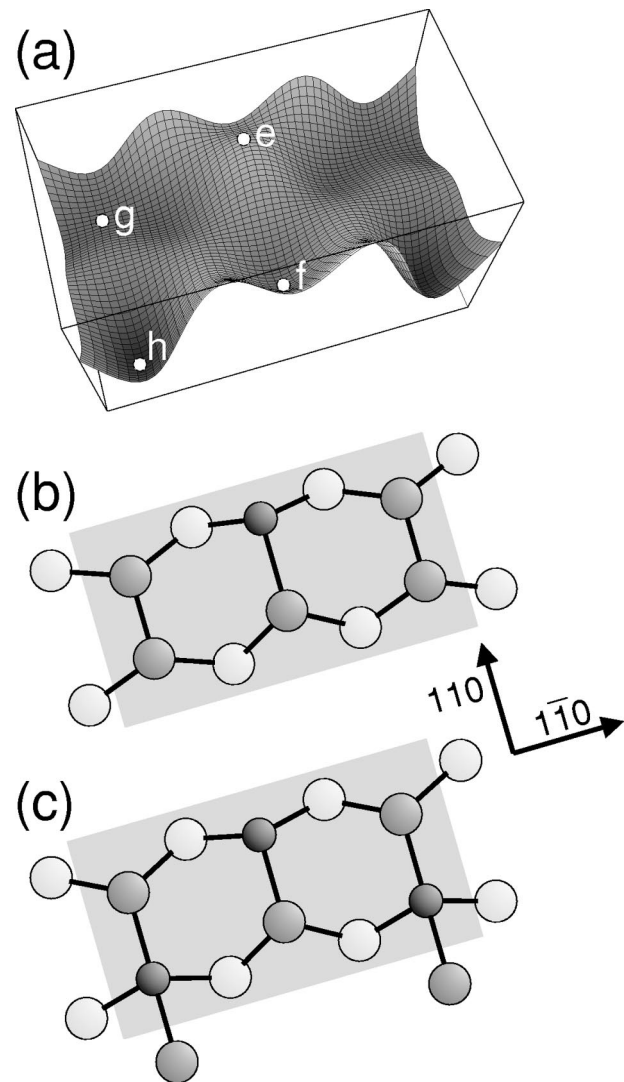


FIG. 7. (a) Potential energy surface for Fe on Fe/GaAs(001), calculated with spin polarization. (b) The initial preadsorbed surface structure, consisting of Fe-Ga heterodimers alternating with Ga dimers. (c) Lowest-energy configuration for 1/2-monolayer-Fe coverage, corresponding to the second Fe adsorbate at point (h) in the potential-energy surface. The shaded area marks the region plotted in (a).

ing that formation of Fe-Ga heterodimers remains favorable for the preadsorbed surface. The global minimum, point (h), corresponds to the staggered arrangement of Fe-Ga heterodimers shown in Fig. 7(c). Occupying all of these adsorption sites results in an Fe coverage of 1/2 monolayer.

Although we do not explicitly calculate energy surfaces for higher coverages, we can make plausible inferences for their basic features based on the PES of Fig. 7. Even for a surface completely terminated by Fe-Ga heterodimers, the strong preference for Fe to form backbonds to As—as evidenced by the local minimum labeled (f) in Fig. 7(a)—should persist. Thus we speculate that continued deposition of Fe will ultimately lead to Fe-Fe dimers atop the As-terminated substrate. An obvious consequence of such a configuration would be the release of Ga (a full monolayer in

this surface model). Moreover, in Sec. III we will show that for Fe films of several monolayers, a floating Ga (or As) adlayer can act as a surfactant, lowering the surface energy by as much as 2 eV/(1×1) cell.

To conclude this section, we have shown that the initial stages of adsorption of Fe are dominated by strong local Fe-As chemistry. For a surface terminated by Ga, this chemistry leads to facile breaking of surface Ga dimers by sequential kicking-out of the two Ga atoms, first forming Fe-Ga heterodimers and, finally, surface Fe dimers bonded to sub-surface As. Excess Ga may be released as a result of this rebonding mechanism. Magnetism plays an auxiliary role in the process by lowering the potential-energy barriers to breaking apart surface Ga dimers. Since the formation of Fe-As bonds leads to efficient trapping of Fe—especially if the excess Ga diffuses away—surface diffusion of Fe will probably be strongly suppressed.

III. GROUND-STATE INTERFACE STRUCTURE

As a complementary approach to the study of single Fe adsorption and diffusion, we have studied epitaxial interfaces of Fe/GaAs. In this section, our focus is threefold: (1) to determine the stability and magnetic character of Fe films for different interface structures and film thickness; (2) to investigate the role of As or Ga adlayers on Fe films, in particular the extent to which they may account for the observed out-diffusion of substrate atoms to the surface; and (3) to examine the possibility of antiferromagnetic order as the origin of the observed magnetic quenching of Fe films with thicknesses of just a few monolayers.

The Fe/GaAs interface structures considered in this section are shown in Fig. 8 for the the As-terminated GaAs(001) interface. Model A is an atomically abrupt interface of bcc Fe and zinc-blende GaAs. Because the lattice constant of bcc Fe ($a = 2.866 \text{ \AA}$) is almost half that of the substrate ($a = 5.654 \text{ \AA}$), the epitaxial relationship is Fe(001) $\langle 100 \rangle$ ||GaAs(001) $\langle 100 \rangle$ and the atomic density of each Fe layer is twice that of the substrate layer, with a strain of only 1.3%. With respect to the bcc Fe lattice, there are vacancy sites in the adjacent GaAs lattice. Models B and C are built by filling these vacancy sites with Fe atoms one by one; we will refer to these interfaces as “partially intermixed” and “fully intermixed,” respectively. For each of these models, we considered film thicknesses ranging from 0.5 ML [one Fe atom per (1×1) of GaAs(001)] up to 3.5 ML. We also considered three analogous models for the Ga-terminated interface. Both As- and Ga-terminated interface models may have relevance for experiments with the more commonly used Ga-rich surfaces: for example, we have already seen in the previous section that substitutional displacement of Ga on a Ga-rich surface leads to an As-terminated Fe/GaAs interface.

For the calculations in this section we again used the GGA, here with an ultrasoft pseudopotential²⁶ for Fe. The electronic wave functions and densities were described by a plane-wave basis with cutoff energies of 16 Ry and 160 Ry, respectively. For each structural model, six or seven atomic

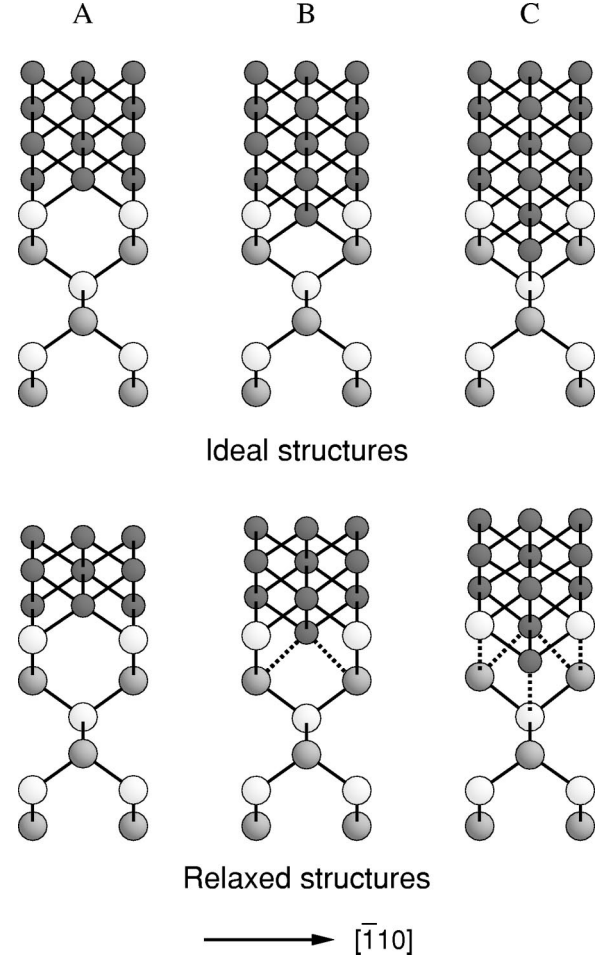


FIG. 8. Interface structures for the As-terminated Fe/GaAs(001) interface: ideal (upper panel) and relaxed structures (lower panel). The gray and light gray spheres represent Ga and As atoms, and the dark gray spheres represent Fe atoms. Highly strained bonds (15%–20% longer than ideal) are shown as dotted lines.

layers were used for the substrate; the bottom As or Ga layer was passivated by pseudohydrogen atoms and fixed during the structural relaxation. The relative stability of each slab is given by its formation energy

$$E_{\text{form}}^{\text{slab}} = E_t - \sum_i N_i \mu_i, \quad (1)$$

where E_t is the total energy of the slab, N_i the number of atoms of each chemical type, and μ_i their chemical potentials. To eliminate the contribution of the pseudohydrogen layer to the formation energy, we define the formation energy of each structural model with respect to a common reference structure,

$$E_{\text{form}}^{\text{model}} = E_{\text{form}}^{\text{slab}} - E_{\text{form}}^{\text{ref}}/2. \quad (2)$$

The reference structure is an ideal GaAs slab passivated on both sides (hence the factor 1/2) by pseudohydrogen atoms. Assuming the thermodynamic equilibrium condition $\mu_{\text{GaAs}} = \mu_{\text{As}} + \mu_{\text{Ga}}$ and taking μ_{GaAs} and μ_{Fe} from bulk structures,

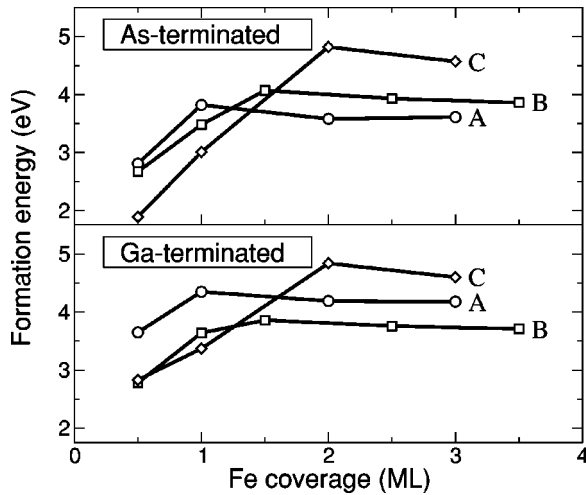


FIG. 9. Formation energies [in eV/(1×1) cell] of Fe films on the GaAs(001) surface given as a function of interface structure (A,B,C) and Fe coverage. The formation energies given are taken at the center of the thermodynamically allowed range of the As chemical potential: in the As-rich limit condition the formation energies decrease (increase) by 0.16 eV for the As-terminated (Ga-terminated) Fe/GaAs interface.

the formation energy is expressed as a function of μ_{As} only within the thermodynamically allowed range $\mu_{\text{GaAs}} - \mu_{\text{Ga(bulk)}} < \mu_{\text{As}} < \mu_{\text{As(bulk)}}$. Here, the lower (upper) limit corresponds to the Ga-rich (As-rich) environment, and $\mu_{\text{Ga(bulk)}}$ and $\mu_{\text{As(bulk)}}$ are again determined from their bulk structures.

Figure 9 shows the calculated formation energies as a function of Fe film thickness. We first discuss Fe films with the As-terminated interface. At a Fe coverage of 0.5 ML model C is most stable, while models A and B are ~ 1 eV higher. This energetic ordering persists up to 1 ML coverage, but changes above that point: the formation energy of model C increases by 1.8 eV from 1 ML to 2 ML, while that of the A and B become nearly independent of coverage. After the formation of 2 ML, the formation energy of all three models does not change much by adding more Fe layers. Thus, the low-energy interface structure turns out to be model A—the abrupt interface. For Fe films with the Ga-terminated interface, a similar trend applies but with a different outcome. At 0.5 ML, models B and C are equally stable, and at 1 ML model C is in fact the most stable. With additional Fe layers, model C becomes very unstable, similar to the case of the As-terminated interface. At higher coverages, however, model B—the partially mixed interface—is most stable.

These results can be understood as a competition between maximizing the coordination of Fe atoms and minimizing the concentration of atoms in the interfacial region. At low Fe coverage (≤ 1 ML), model C is energetically most favored, because Fe atoms can maximize their coordination with substrate atoms. At higher coverages, where the interface is well defined, this arrangement becomes unstable relative to the less intermixed interfaces. The reason for this crossover is the two extra Fe atoms per (1×1) surface cell (relative to model A). The excess electrons from the extra Fe atoms fill antibonding orbitals and thus weaken the interface bonding.

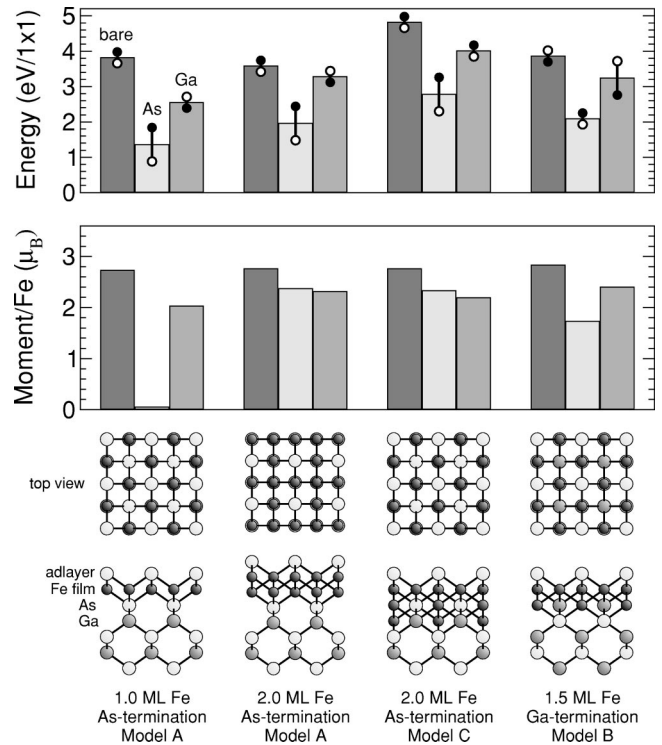


FIG. 10. Formation energies and magnetic moments for four selected adlayer structures. The Fe film thickness, substrate termination, and interface model are listed underneath each structure. Formation energies and magnetic moments are shown for bare Fe films and for As and Ga adlayers. The formation energies are calculated at the center of the thermodynamically allowed range of the As chemical potential (μ_{As}). The changes at the limiting values of μ_{As} are indicated by small circles (solid circles correspond to the Ga-rich limit, open circles to the As-rich limit).

This weakened bonding is also evident in the relaxed interface separations: for both As- and Ga-terminated interfaces, the position of the first Fe monolayer is ~ 0.8 Å higher in model C and ~ 0.4 Å higher in model B, compared to model A (see the relaxed structures in Fig. 8). Similar reasoning explains why model B is more stable than model A for the Ga-terminated interface, while the opposite holds for the As-terminated interface.

The present results emphasize that the low-energy atomic structure at low Fe coverage may not be extrapolated to high coverages. This should be true also in real growth situations, since Fe atoms at low coverages would take positions one or two layers deep so as to maintain maximal coordination. Further deposition of Fe leads to a partially mixed interface that ultimately becomes unstable. Therefore, it is likely that substantial rearrangement of the atomic structure occurs during the film growth, provided the temperature is sufficiently high. This may partly account for the experimental observation^{22,27,28} that substrate atoms, especially As atoms, diffuse out to the surface during the Fe growth even for room-temperature deposition.

To follow this reasoning, we examined the effect of a Ga or As adlayer on top of the Fe film. In Fig. 10 we compare the formation energies of four selected interface structures with and without an adlayer. Both Ga and As adlayers stabi-

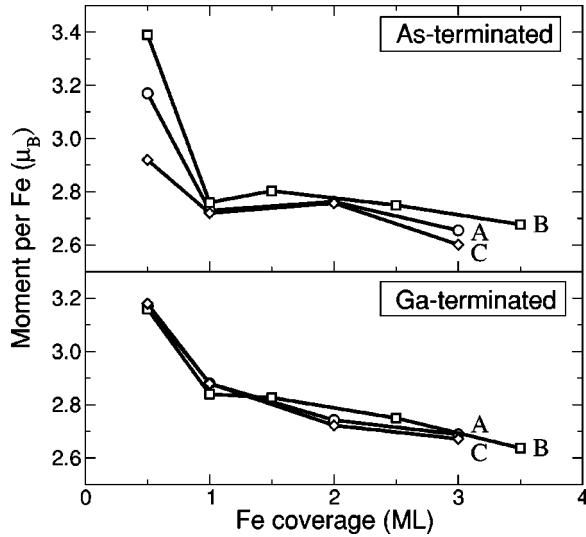


FIG. 11. Magnetic moments of Fe films on GaAs(001) as a function of interface type and Fe coverage.

lize the surface substantially, regardless of the interface structure and film thickness. This is not surprising, since adlayers increase the coordination of surface Fe atoms. The energy gain from As adlayers is particularly large, amounting to more than $1.5 \text{ eV}/(1 \times 1)$ in most cases. Adlayers on 1 ML of Fe show strong dependence on the adatom site: the low-energy site is the position extended from the substrate GaAs lattice, suggesting a strong covalent bonding between the substrate and the adlayer, mediated by the intervening Fe layer.

The results for adlayer structures, together with the interface energetics, provide strong theoretical evidence that substitutional adsorption and/or atomic exchange is an essential process during the Fe growth—a finding which was anticipated by experiments²⁷ and which we explicitly demonstrated in Sec. II. By substitutional adsorption processes, Fe atoms can maximize their coordination at every stage of the growth. These processes result in the segregation of substrate atoms to the surface and simultaneously facilitate optimal interfacial atomic densities and thus relatively stable interface structures. Our calculations have shown that such processes are inevitable and that the energy gain from them is quite substantial.

We now turn to magnetic properties of the interface structures. Calculated spin moments (per Fe atom) of various model structures are given in Figs. 10 and 11. For bare Fe films without Ga or As adlayers, average Fe spin moments are much enhanced compared to the calculated bulk value for Fe of $2.33 \mu_B$. Figure 11 shows that for films of 3 ML this enhancement is still substantial and relatively insensitive to the specific interface structure or substrate termination. For Fe films with adlayers, Fig. 10 shows that both As and Ga adlayers suppress total magnetic moments, by as much as $1 \mu_B$ in several cases.

In order to examine local variations in the total magnetic moments, we calculated partial moments within a sphere centered on each atom, in analogy to the muffin-tin sphere in all-electron approaches. We used a sphere radius of 1.2 \AA ,

TABLE I. Atom-resolved spin moments (in μ_B) for Fe/GaAs interface structures. The layer number is given with respect to the top substrate layer. The induced spin moments of substrate atoms are given with a species label.

Layer	As:A 3.0 ML	Ga:B 3.5 ML	As:A2.0 ML \ As
3	3.03, 3.00	3.02, 2.99	-0.08 (As)
2	2.51, 2.38	2.49, 2.43	2.52, 2.42
1	2.54, 2.49	2.49, 2.42	2.40, 2.29
0	-0.04 (As)	2.72, -0.06 (Ga)	-0.04 (As)
-1	0.02 (Ga)	0.00 (As)	0.02 (Ga)
-2	0.01 (As)	0.03 (Ga)	0.02 (As)
-3	0.00 (Ga)	0.01 (As)	0.00 (Ga)

which is slightly shorter than the minimum bond length between atoms. Table I shows the results for three selected structures. Local Fe moments are significantly enhanced ($\sim 3.0 \mu_B$) at the surface layer. For the relatively thin Fe films considered in this work, the buried and interfacial Fe layers also have sizable enhancement. The adlayer suppresses spin moments not only of the top-layer Fe atoms but also slightly of the second-layer Fe atoms. Both the enhancement and suppression can be understood in terms of changes in the Fe d -band width due to changes in coordination and symmetry. On the other hand, substrate atoms have small induced moments up to 3–4 layers deep, always with negative spin moments for the interfacial atoms. The sign of spin moments changes to positive at deeper layers, suggesting the formation of a spin-density wave.

Recent magnetic measurements have observed a delayed onset of the magnetic phase at $\sim 2 \text{ ML}$ for Fe films grown on the Ga-rich GaAs(001)- (2×6) and (4×2) surfaces.²⁹ Of the various surface structures we have considered here, one shows a similar quenching effect. The As-terminated interface with 1 ML of Fe (the first structure in Fig. 10) has a zero net moment when capped by an As adlayer. Since this structure also has the lowest formation energy for an Fe coverage of 1 ML, it might be anticipated that the delayed onset is due to the quenching of magnetism from the strong covalent bonding between the As atoms via Fe atoms. However, there is another possibility: namely, the formation of antiferromagnetic (AF) order. We have considered the possibility of AF order for the simplest structures with 1 ML of Fe in the same plane, so that one Fe atom has spin up and the other down. The results, summarized in Fig. 12, indicate that films with an As adlayer become more stable by $0.05-0.09 \text{ eV}/(1 \times 1)$ upon the formation of AF order, while bare films and films with a Ga adlayer become unstable by $0.2-0.5 \text{ eV}/(1 \times 1)$. We note that the lowest-energy structure with quenched magnetism is unstable toward AF order. We propose on this basis that the observed delayed magnetic onset is due to the initial formation of AF order and tightly correlated with the outdiffusion of As atoms to the surface.

While the microscopic origins driving the formation of AF order are not clear in detail, it appears that the surface As atoms mediate the AF order between Fe atoms. A related

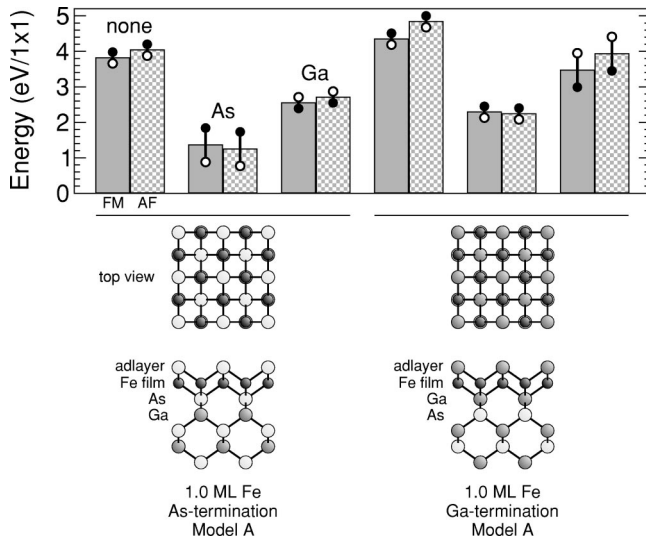


FIG. 12. Formation energies of ferromagnetic (FM) and antiferromagnetic (AF) Fe films in two different Fe/GaAs structures (As- and Ga-terminated abrupt interfaces). Three types of adlayers are considered (none, As, Ga).

observation is that the AF-stabilized surface structure is locally similar to the tetragonal Fe_2As structure in the AF ground state: the unit cell consists of bimolecular units with two Fe atoms in the same plane, plus one As and one Fe atom on each side of the Fe plane.³⁰ Thus it is plausible that AF order in Fe/GaAs interfaces at low coverage arises from the formation of the Fe_2As -like structures. This local similarity is broken by additional Fe adsorption, so that ferromagnetic order is ultimately favored.

To conclude this section, we have shown that the low-energy interface structure is different for low and high Fe coverages. The addition of Ga or, especially, As adlayers substantially lowers the surface formation, providing a theoretical basis for the experimentally observed outdiffusion of substrate atoms to the surface. We have shown that Fe films on the GaAs substrate usually assume a ferromagnetic ground state even at very low coverages, while for certain cases an As adlayer can induce antiferromagnetic order in the Fe film. Since the latter cases generally have lower formation energies and are thus likely to form, we propose that the observed magnetic quenching for very low Fe coverage may be due to the formation of antiferromagnetic order.

IV. SUMMARY AND FUTURE DIRECTIONS

We have taken two complementary approaches to understanding the nucleation and growth of Fe on GaAs—one focusing on the behavior of single Fe adatoms deposited on clean and partially preadsorbed GaAs(001), the other focusing on the interface structure of complete Fe films at coverages up to several monolayers. Although a detailed growth history of Fe/GaAs interfaces cannot yet be described, our studies suggest four generic features that may play an important role.

First, for low coverages we have identified a very strong

driving force for Fe to be highly coordinated. For single adatoms, this tendency is strong enough to spontaneously break surface Ga-Ga and Ga-As bonds in order to form Fe-As bonds. Although magnetic effects do not dominate this chemistry, they play an interesting auxiliary role by essentially removing energetic barriers from the reaction pathways. For half-monolayer films constrained by symmetry, these local surface chemical reactions are not possible, and the Fe atoms respond by occupying subsurface sites with high coordination to either Ga or As.

A second generic feature is the crossover from a preference for strongly intermixed films to less intermixed or even abrupt films. This crossover occurs between one and two ML for both As- and Ga-terminated interfaces. Its origin is not magnetic: the films exhibit moments per atom larger than the bulk value even for very low coverages, and the moments converge to their bulk value long after the crossover occurs. Rather, it arises from the competition between maximizing the coordination of Fe atoms (which favors intermixing) and minimizing the amount of excess interfacial Fe (which favors abrupt interfaces). For well-defined Fe films of 2 ML or more, the latter effect dominates and sharper interfaces become energetically preferred.

A third finding, common to all interfaces we have studied, is that Ga and As adlayers dramatically reduce the formation energies of Fe films. This stabilizing effect occurs for both Ga- and As-terminated interfaces, for both intermixed and abrupt interfaces, and for all film thicknesses considered. It is especially striking for As adlayers, which can reduce the film formation by as much as 50%. We also find that this stabilization is generally accompanied by a suppression of the total magnetic moment of the film; since this is due to reduced local moments in the topmost layer or two, the effect is largest for thinner films. Indeed, for 1-ML Fe films with an As adlayer, antiferromagnetic order can be more stable than ferromagnetic order.

Taken together, these three generic features collectively imply a fourth: the diffusion of Ga or As atoms from the interface to the surface of the Fe film. We have shown explicitly how Ga can be released by adsorption of individual Fe adatoms and the subsequent “kick-out” of Ga from surface dimers. Even for GaAs surface reconstructions that do not consist of Ga dimers,²³ we speculate that the same strong Fe-As chemistry would again lead to the release of surface Ga atoms. We have also shown that during the growth—between 1 and 2 ML—a spontaneous rearrangement of the interface morphology is likely to occur, again leading to the release of either Ga or As. Although we do not speculate about the details of this atomic rearrangement, we have also shown that ultimately the liberated Ga or As is likely to play the role of a floating surfactant layer.

Finally, we mention a possible avenue for further research. One difficulty with theoretical studies of interface is the paucity of macroscopic observables that can be directly related to the microscopic interface structure. Schottky barriers are extremely sensitive probes of interface structure, varying by as much as 25% for local changes in interface geometry.³¹ Schottky barrier heights have been measured in Fe/GaAs interfaces to be of order 0.7 eV (Ref. 32) and thus

represent a useful probe of interface microstructure. Moreover, Schottky barriers may actually be a necessary ingredient for circumventing the intrinsic limitations on spin injection from a ferromagnetic metal into a semiconductor. A theoretical understanding of their dependence on Fe/GaAs interface structure—including substrate termination and reconstruction, degree of intermixing, and magnetic character—would be a great asset.

ACKNOWLEDGMENTS

This work was funded in part by ONR and in part by the Deutsche Forschungsgemeinschaft. Computational work was supported in part by a grant of HPC time from the DOD Major Shared Resource Center ASCWP. S.C.E. and S.H.L. acknowledge generous support from the Alexander von Humboldt Foundation.

*Permanent address: Computational Science and Engineering Center, Samsung Advanced Institute of Technology, P. O. Box 111, Suwon 440-600, South Korea.

¹G.A. Prinz, *Science* **282**, 1660 (1998)

²R. Fiederling, M. Keim, G. Reuscher, W. Ossau, G. Schmidt, A. Waag, and L.W. Molenkamp, *Nature (London)* **402**, 787 (1999).

³B.T. Jonker, Y.D. Park, B.R. Bennett, H.D. Cheong, G. Kioseoglou, and A. Petrou, *Phys. Rev. B* **62**, 8180 (2000).

⁴Y. Ohno, D.K. Young, B. Beschoten, F. Matsukura, H. Ohno, and D.D. Awschalom, *Nature (London)* **402**, 790 (1999).

⁵C. Haas, *IBM J. Res. Dev.* **14**, 282 (1970).

⁶G.A. Prinz and J.J. Krebs, *Appl. Phys. Lett.* **39**, 397 (1981).

⁷P.R. Hammar, B.R. Bennett, M.J. Yang, and M. Johnson, *Phys. Rev. Lett.* **83**, 203 (1999).

⁸Y.B. Xu, D.J. Freeland, E.T.M. Kernohan, W.Y. Lee, M. Tselepi, C.M. Guertler, C.A.F. Vaz, J.A.C. Bland, S.N. Holmes, N.K. Patel, and D.A. Ritchie, *J. Appl. Phys.* **85**, 5369 (1999).

⁹J.J. Krebs, B.T. Jonker, and G.A. Prinz, *J. Appl. Phys.* **61**, 2596 (1987).

¹⁰A. Filipe, A. Schuhl, and P. Galtier, *Appl. Phys. Lett.* **70**, 129 (1997).

¹¹G.W. Anderson, M.C. Hanf, and P.R. Norton, *Phys. Rev. Lett.* **74**, 2764 (1995).

¹²M. Zöfl, M. Brockmann, M. Kohler, S. Kreuzer, T. Schweinbock, S. Miethaner, F. Bensch, and G. Bayreutherp, *J. Magn. Magn. Mater.* **175**, 16 (1997).

¹³E.M. Kneedler and B.T. Jonker, *J. Appl. Phys.* **81**, 4463 (1997).

¹⁴Y.B. Xu, E.T.M. Kernohan, D.J. Freeland, A. Ercole, M. Tselepi, and J.A.C. Bland, *Phys. Rev. B* **58**, 890 (1998).

¹⁵G. Schmidt, D. Ferrand, L.W. Molenkamp, A.T. Filip, and B.J. van Wees, *Phys. Rev. B* **62**, R4790 (2000).

¹⁶H.X. Tang, F.G. Monzon, R. Lifshitz, M.C. Cross, and M.L. Roukes, *Phys. Rev. B* **61**, 4437 (2000).

¹⁷E.I. Rashba, *Phys. Rev. B* **62**, R16267 (2000).

¹⁸A. Hirohata, Y.B. Xu, C.M. Guertler, and J.A.C. Bland, *J. Appl. Phys.* **87**, 4670 (2000).

¹⁹H.J. Zhu, M. Ramsteiner, H. Kostial, M. Wassermeier, H.-P. Schönherr, and K.H. Ploog, *Phys. Rev. Lett.* **87**, 016601 (2001).

²⁰A.T. Hanbicki, B.T. Jonker, G. Itskos, G. Kioseoglou, and A. Petro, *Appl. Phys. Lett.* **80**, 1240 (2002).

²¹P. Kratzer and M. Scheffler, *Comput. Sci. Eng.* **3**, 16 (2001).

²²E.M. Kneedler, B.T. Jonker, P.M. Thibado, R.J. Wagner, B.V. Shanabrook, and L.J. Whitman, *Phys. Rev. B* **56**, 8163 (1997).

²³S.H. Lee, W. Moritz, and M. Scheffler, *Phys. Rev. Lett.* **85**, 3890 (2000).

²⁴J.P. Perdew, J.A. Chevary, S.H. Vosko, K.A. Jackson, M.R. Pederson, D.J. Singh, and C. Fiolhais, *Phys. Rev. B* **46**, 6671 (1992).

²⁵M. Bockstedte, A. Kley, and M. Scheffler, *Comput. Phys. Commun.* **107**, 187 (1997).

²⁶D. Vanderbilt, *Phys. Rev. B* **41**, 7892 (1990).

²⁷S.A. Chambers, F. Xu, H.W. Chen, I.M. Vitomirov, S.B. Anderson, and J.H. Weaver, *Phys. Rev. B* **34**, 6605 (1986).

²⁸T.L. Monchesky, B. Heinrich, R. Urban, K. Myrtle, M. Klaua, and J. Kirschner, *Phys. Rev. B* **60**, 10 242 (1999).

²⁹F. Bensch, G. Garreau, R. Moosbuhler, G. Bayreuther, and E. Beaurepaire, *J. Appl. Phys.* **89**, 7133 (2001).

³⁰R. W. G. Wyckoff, *Crystal Structures*, 2nd ed., (Interscience, New York, 1963), Vol. 1, p. 360.

³¹D.R. Heslinga, H.H. Weitering, D.P. van der Werf, T.M. Klapwijk, and T. Hibma, *Phys. Rev. Lett.* **64**, 1589 (1990).

³²J.A.C. Bland, A. Hirohata, C.M. Guertler, Y.B. Xu, and M. Tselepi, *J. Appl. Phys.* **89**, 6740 (2001).